Acta Geochimica (2023) 42:471–487
https://doi.org/10.1007/s11631-023-00596-9

ORIGINAL ARTICLE

Petrogenesis of the Neoarchean zincian chromite within ultramafic xenoliths, Bastar Craton, India

Arpita Karmakar[1] · Tushar Meshram[2] · Mohammad Asif[3] · Yogesh Pandey[3]

Received: 17 October 2022 / Revised: 8 January 2023 / Accepted: 10 January 2023 / Published online: 15 February 2023

Abstract The present study reports and discusses the genesis of zincian chromite in the ultramafic xenoliths from the Dongripali area, Bastar craton, Central India. The zincian chromite is in the ultramafic xenoliths of Bengpal supracrustal rock hosted by Neoarchaean Bundeli gneisses. Compositionally zincian chromite shows a range of Cr_2O_3 (39.69 to 51.66 wt%), Al_2O_3 (05.30 wt% to 08.71 wt%), FeO (21.74 wt% to 27.51 wt%), Fe_2O_3 (10.19 wt% to 19.36 wt%) with higher ZnO content ranging from 1.73 wt% to 4.08 wt%. Accordingly, their Cr# [Cr/(Cr + Al)] varies in a narrow range from 0.83 to 0.85. Its calculated melt composition supports metamorphic or post-magmatic nature rather than common occurrences such as inclusion in diamonds, meteorites, and association with any sulfide-rich mineralised belt. This reveals that the post-magmatic processes play a vital role in transforming chromite to zincian chromite. The empirical thermometric calculation from chromite, amphibole, and pyroxene support their metamorphic origin and formed during low-P and high-T amphibolite grade facies of metamorphism (~ 700 °C). The Neoarchaean granitic magmatism has a significant role in generating and transferring the heat during contact metamorphism with hydration of ultramafic xenoliths and further alteration, i.e., serpentinisation. The olivine is a major repository for Mn, Zn, and Co in peridotite/ultramafic; these elements get mobilised during the metamorphism and serpentinisation. This is a possible reason for the mobilisation of zinc and incorporation in the chromite within altered ultramafic. As a result, chromite-rich ultramafic xenolith subjected to metamorphic process gets enrichment of Zn and Fe due to elemental exchange. It converts common chromite into zincian chromite, as reported in altered ultramafics elsewhere.

Keywords Zincian chromite · Ultramafic · Neoarchaean granitic magmatism · High-grade metamorphism

1 Introduction

Chromite is a common mineral in the layered mafic–ultramafic, ophiolite, and Alaskan-type complex. However, chromium concentration has been reported from sedimentary and metamorphic terrains, i.e., laterite and saprolite derived from ultrabasic rocks, beach placer and metamorphosed limestones, serpentinites many times host chromium-bearing minerals (Dill 2010 and reference therein). Chromite from igneous rocks has been widely used as a petrogenetic indicator in magmatic environments (Irvine 1965 1967; Hill and Roeder 1974; Sack et al. 1991; Arai 1992, Arai et al. 1994; Roeder 1994; Barnes et al. 2001; Kamenetsky et al. 2001) because its composition depends on the degree of fractional crystallisation of the parental melt and the extent of partial melting experienced by the mantle source (Maurel and Maurel 1982; Kamenetsky et al. 2001; Dick and Bullen 1984; Arai et al. 1994; Roeder 1994; Barnes and Roeder 2001; González-Jiménez et al. 2013). It also plays a significant role in understanding the potential of Fe − Ni − Cu − Co sulfide and PGE mineralisation in the above-mentioned complexes (Groves et al.

✉ Arpita Karmakar
geotinni@gmail.com

[1] Geological Survey of India, Vasudha Bhawan, Kumarswamy Layout, Bangalore 560111, India

[2] Geological Survey of India, Nagpur, India

[3] Geological Survey of India, Raipur, India

1983; Paktunc and Cabri 1995; Fanlo et al. 2015; Evans 2015, 2017; Meshram 2020; Meshram et al. 2022). This suggests that many factors must be considered, particularly chromite's tendency to re-equilibrate with surrounding silicates during prolonged cooling and metamorphism (Barnes and Roeder 2001).

Zinc is one of the principal ores associated with polymetallic deposits that form in magmatic, metamorphic, and sedimentary lead–zinc deposits (Dill 2010 and reference therein). In these systems most common mineral for zinc is sphalerite, nonsulphidic zinc minerals like zincian spinel-franklinite, gahnite, zinc silicates (willemite, zincian staurolite), and oxides (zincite) are present in metamorphosed zinc-polymetallic deposits (Dill 2010; Dill et al. 2021). In contrast, zinc concentrations in chromite are quite uncommon compared to magnesium (Mg) and iron (Fe). Accordingly classified as, magnesiochromite [$(MgAlCr)_2O_4$], ferrit chromite [$(FeAlCr)_2O_4$] and zincian chromite [$(ZnAlCr)_2O_4$]. Zinc concentration in chromite appears to be susceptible to subsolidus re-equilibrations that are controlled not only by the temperature but also by the distribution of the dominant divalent cations in chromian spinel (Paktunc and Cabri 1995). Several studies reported that the enrichment of zinc content within chromite either as a result of elemental re-distribution or substitution with associated silicates during high-grade metamorphism (> 500 °C, upper amphibolite facies) (Arai et al. 1998; Barnes and Roeder 2001; Gahlan and Arai 2007; Arai and Ishimaru 2011; Matsumoto et al. 2017; Dill et al. 2021) or the role of mineralising fluids rich in Zn-, Mn- and Co content and Ni–sulfide deposits those that are enclosed or adjacent to sulfides display higher Zn contents (Groves et al. 1983; Fanlo et al. 2015). In contrast, zincian chromite also occurs as primary inclusion in diamonds obtained from kimberlites and lamprophyres, the origin of these inclusions is possibly deep recycling of peridotites that generate the kimberlitic magma (Armstrong and Barnett 2003; Johan and Ohnenstetter 2010; Arai and Ishimaru 2011). The next and last possibility of the formation of zincian chromite is particularly common in silicate inclusions in iron meteorites and rarely in achondrites (e.g., Bunch et al. 1970; Chikami et al. 1999). The zincian chromite extremely rare detrital occurrences reported from gold-bearing meta-conglomerates of the Paleoproterozoic Tarkwaian Group of Ghana (Weiser and Hirdes 1997), in Banded Chromite Quartzite/Fuchsite Quartzite (BCQ/BCFQ) from Ghutrigaon area, Dhenkanal district, Odisha, eastern India in closed proximity to the two well-known Sukinda and Boula-Nuasahi chromite deposits (Das et al. 2021) and other metasedimentary rocks or volcano sediments (Dill 2010 2021).

This study reports the zincian chromite from the ultramafic xenoliths within Bengpal gneisses in the Dongripali area, Bastar craton, Central India is part of the Bengpal Group of rocks, which occurs close vicinity to Sonakhan Greenstone Belt (SGB). These ultramafic xenoliths suffered regional deformation and metamorphism. The occurrence of chromite within olivine and clinopyroxene cumulates previously reported from SGB (Manu Prasanth et al. 2018). The SGB chromite has a different composition than the present study's chromite. The significant compositional variation in zincian chromite within the ultramafic xenolith further supports the multiple changes that occur during post-magmatic events, i.e., regional metamorphism. The present study emphasises the enrichment of zinc content in chromite within these ultramafic xenoliths, which can be used to understand the involvement of different post-magmatic processes in different geodynamic settings operated in the northeastern part of the Bastar craton during its evolution.

2 Regional geological setting

The Bastar craton (BC) of Central India comprises cratonic components spanning from Mesoarchean to Neoproterozoic in age (Santosh et al. 2020) (Fig. 1A). The older basement gneisses cover the major part of the BC. This older basement gneiss of the Bastar craton has been dated by U–Pb zircon dating, indicating the age of 3509 ± 14 Ma (Sarkar et al. 1993) and 3561 ± 11 Ma (Ghosh 2004), which implies that the Bastar craton was a component of the earliest part of Indian Shield (Sarkar et al. 1993; Ghosh 2004; Rajesh et al. 2009; Santosh et al. 2020). It is surrounded by tectonic belts of various ages, which include the Bengpal-Sukma belt in the south, Kotri-Dongargarh belt in the centre, Amgaon belt in the west, Sausar-Chilpi belt in the north, and Sonakhan belt in the east. The SGB is located on the northeastern fringes of Bastar Craton and is almost perpendicular to the NE–SW trending Central Indian Tectonic Zone (Fig. 1B) (Manu Prasanth et al. 2017). These supracrustals are intruded by Mesoarchean gneisses (also known as Bengpal/Baya/Sukma gneisses of 3081 ± 60 Ma age, Sarkar et al. 1993) and numerous Proterozoic granites (i.e., Dongargarh granite, Bundeli Granitoid and Malanjkhand of ~ 2500 Ma ages, Sarkar et al. 1993; Stein et al. 2004), which was followed by intrusive mafic magmatic dike swarms (1891−1883 Ma, French et al. 2008). These gneisses/granites also contain the xenoliths of supracrustals, i.e., Sukma and Bengpal Group of rocks, which vary in size from a few meters to kilometres and are inhomogeneously distributed in the area (Fig. 1B). This granite magmatism in Bastar craton show similarity with a widespread Closepet granitic magmatism (2.51 Ga) occur between eastern Dharwar craton (EDC) and western

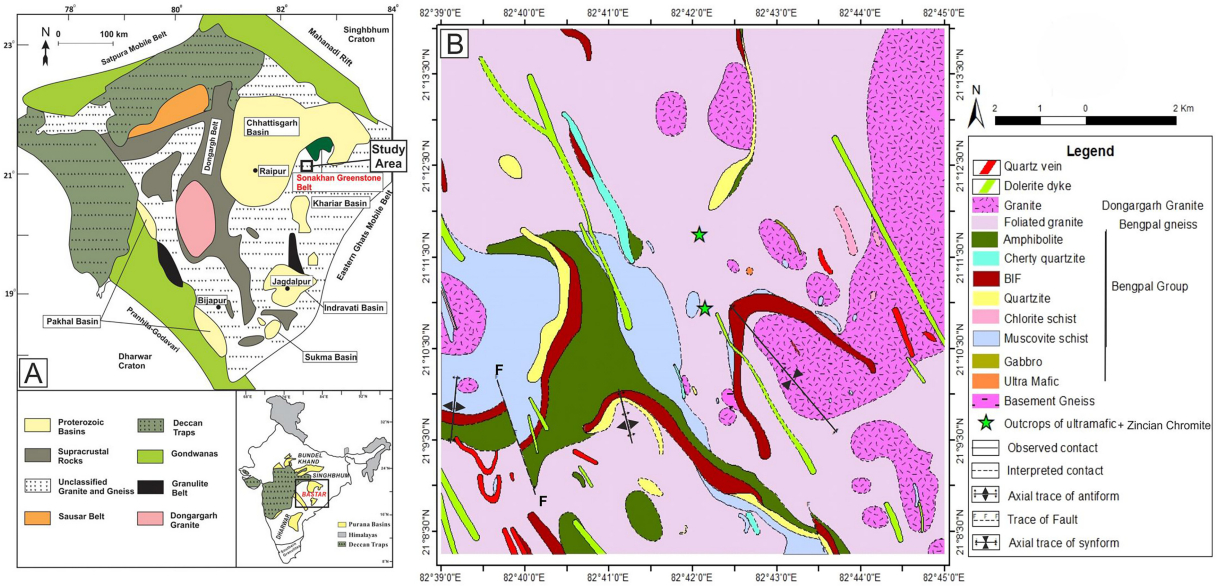

Fig. 1 **A** Generalised geological map of Bastar craton shows Sonakhan Greenstone Belt's location. The inset map is the generalised geology of the Indian subcontinent showing Bastar craton (modified after Meert et al. 2010 and Manu Prasanth et al. 2017). **B** Geological map showing zincian chromite-rich ultramafic xenolith location at the Dongripali area, Bastar craton, Central India (Asif et al. 2018)

Dharwar craton (WDC) (Jayananda et al. 2000) and also with granitic magmatism of Aravalli craton (2.56–2.44 Ga) (Wiedenbeck et al. 1996), which is indicating widespread granite plutonism throughout the Indian Shield at the Archean/Proterozoic boundary. This granitic magmatism is part of global Neoarchaean magmatism in the Indian shield and other parts of the world, followed by high-grade metamorphism. The earlier metamorphic event in the Dharwar craton, southern India reported close to 3.0 Ga by Mahabaleswar and Peucat (1988) and Peucat et al. (1993, 1995). The ca 2.62 Ga granulite assemblages with ultra-high temperature (UHT) conditions reported from Dharwar craton and Southern Granulite Terrain (Rajesham et al. 1993; Santosh et al. 2004; Jayananda et al. 2012), which has spatial links to crustal accretion, regional deformation, cratonization is not well constrained, particularly for pre-2.5 Ga tectonic-metamorphic events. Similarly, the Bastar craton also has older 3.56–3.51 Ga rocks, i.e., TTGs and 2.4 to 2.6 Ga with variable high-grade metamorphism (Sarkar et al.1993; Ghosh 2004; Rajesh et al.2009; Mohanty 2015; Meshram et al. 2021; Dora et al. 2021).

The study area is located in the northeastern part of Bastar craton (BC), Central India (Fig. 1A, B). The present study area dominantly comprises Neoarchean gneiss and intrusive Proterozoic granites, followed by the Bengpal Group of rocks (Fig. 1B). The Bengpal Group of rocks occur as mega-xenoliths within Bengpal gneisses and Bundeli granites. This Bengpal Group of rocks is highly deformed metasedimentary and metabasic rocks mainly consisting of muscovite schist, chlorite schist, fuchsite-quartzite, BIF, cherty quartzite, amphibolite, metagabbro, metapyroxenite. They followed the regional structure with the development of folded mega-xenoliths of Bengpal supracrustals with the NW–SE trending axial plane (Fig. 1B). The metapyroxenite is associated with layered metagabbro near the hinge part of the regional fold. The Bengpal Group is overlaid by the Neo-Proterozoic Sonakhan Group, which is exposed as linear composite lithounits of metamorphosed volcano-sedimentary sequence and a bimodal igneous suite. Metasedimentary rocks of Sonakhan Group include Boulder bed and conglomerate, pebbly schist, pebbly quartzite, mica schist, phyllite, and shale. The secondary quartz veins are the younger intrusive occur in the area.

3 Methodology

Samples were collected from the ultramafic xenolith used for the preparation of polishing thin sections for the identification of chromite mineralisation and detailed petrographic studies of silicate and oxides. From the 05 polished thin sections after detailed petrographic study and scanning in SEM, one sample was selected for the EPMA study, which contains disseminated chromite grain within the ultramafic. The petrographic studies of zincian chromite-rich ultramafic were carried out using LEICA DM RX. After detailed petrographic studies, the section was selected for the EPMA study to know the compositional variation of zincian chromite and silicate minerals. The silicate and oxide phase analyses were performed using a

CAMECA SX-100 electron microprobe analyser. The EMP instrument is equipped with five wavelength dispersive spectrometers (WDS), e.g., WDS 1 (TAP crystal), 2 (PET crystal), and 4 (TAP crystal) fitted with low-pressure detectors, and WDS 3 (LPET crystal) and WDS 5 (LIF) fitted with high-pressure detectors (all detectors use P-10 gas). Polypropylene separation windows were used with WDS 1, 2, and 4, and Mylar windows were used with WDS 3 and 5. Calibration, overlap correction, and quantifications were performed with the CAMECA SX- 100 Peak Sight-Geo Quanta software package. Pulse-height analysers (PHAs) were adjusted by selecting the differential auto mode for all the elements. Matrix effects were eliminated using the X-PHI correction method proposed by Merlet (1992, 1994). Silicate and oxide phases were analysed using 15 kV acceleration voltage and 15 nA beam current with a beam 1 µm size. The signals used are Na Ka, Si Ka, Mg Ka, Al Ka, K Ka, Ca Ka, Ti Ka, Cr Ka, Fe Ka, and Mn Ka for calibration of elements using natural standards for Na, Si, Ca, K, Fe, Mg, Mn, synthetic standards for Al, Ti, Cr. Standards used are jadeite for Na, wollastonite for Si, Ca, diopside for Mg, corundum for Al, orthoclase for K, rutile for Ti, chromite for Cr, haematite for Fe and rhodonite for Mn. The counting time for peak measurement is 10 s and half of the peak measurement time allotted for background measurement.

4 Result

4.1 Petrography

The host rock of the zincian chromite is present as xenolith within Nearchean gneiss. The xenolith is massive and dark green, whereas the altered one is highly friable and yellowish-green in colour (Fig. 2). They are medium to coarse-grained in nature and traverse by criss-cross carbonate vein network (Fig. 2A). This xenolith is mainly pyroxenite in composition, which shows a high degree of alteration and metamorphism. At places, it offers various degrees of alteration due to later hydrothermal activities, which developed yellowish-green colour to the metapyroxenite. The serpentinisation also occurs along the fractures within metapyroxenite at places (Fig. 2B). In contrast, the rest of the rock gets completely serpentinised in some places (Fig. 2C). Though metamorphosed laterite also sometimes contains chromite grains and can occur as xenolith within granite (Dill 2010), the field and petrographic studies reveal the well preserved ultramafic xenolith with serpentinisation at places in the present study area.

The metapyroxenite is medium to coarse-grained, shows a relict primary igneous interlocking texture, and is mainly composed of amphiboles and pyroxenes with disseminated

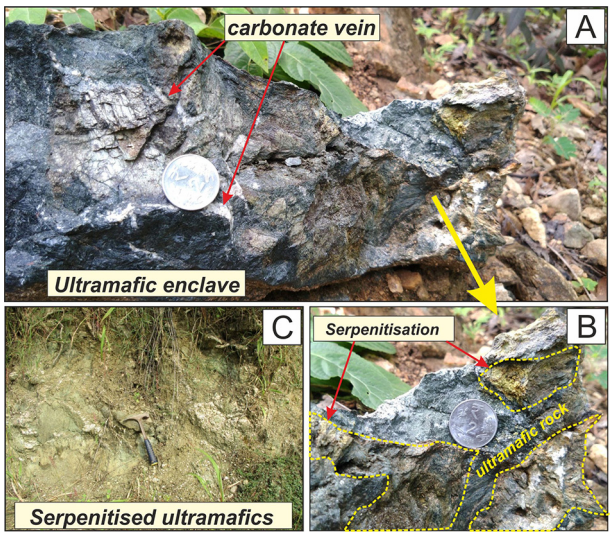

Fig. 2 Representative field photographs showing ultramafic xenolith in the study area. **A** Field photograph showing the dark green colour ultramafic xenolith with partly serpentinisation and traverse by carbonate veins. **B** Close view of field photograph showing the development of serpentinised patches due to alteration within ultramafic. **C** Field photograph showing the yellowish green colour highly altered/ serpentinised ultramafic

chromite grains (Fig. 3A). The pyroxenes are partly altered to amphiboles but, at places, relict and pseudomorph of pyroxenes are preserved. Chromite, pyrrhotite, and chalcopyrite occur as accessory mineral phases. The relict pyroxenes are observed at places with two prominent cleavage sets. The amphibole is dominantly hornblende and anthophyllite in nature, whereas pyroxenes are clinoferrosilite and diopside to hedenbergite in nature. The euhedral chromite grains also occur as fine dissemination within metapyroxenite. They are also occurring as inclusions within pyroxenes and vice-versa. Chromite grains are 5 microns to 60 microns sized, euhedral in shape, and light grey colour with low reflectivity under the oil immersion (Fig. 3D–F).

At places, chromite grain contains small rounded inclusions composed of alumina and silica. The elemental mapping shows the distribution of Al, Si, Mg, Mn, Fe, Cr, and Zn within zincian chromite (Fig. 3G). These elemental maps show homogeneous distribution and enrichment of Fe and Zn within chromite and don't follow any zoning pattern.

4.2 Mineral chemistry

The chromite, pyroxene, and amphibole were analysed using EPMA, and representative analyses are mentioned in Tables 1, 2, and 3. Similarly, the respective backscattered images were taken for textural interpretation in SEM and EPMA, and different elemental mapping in the chromite to

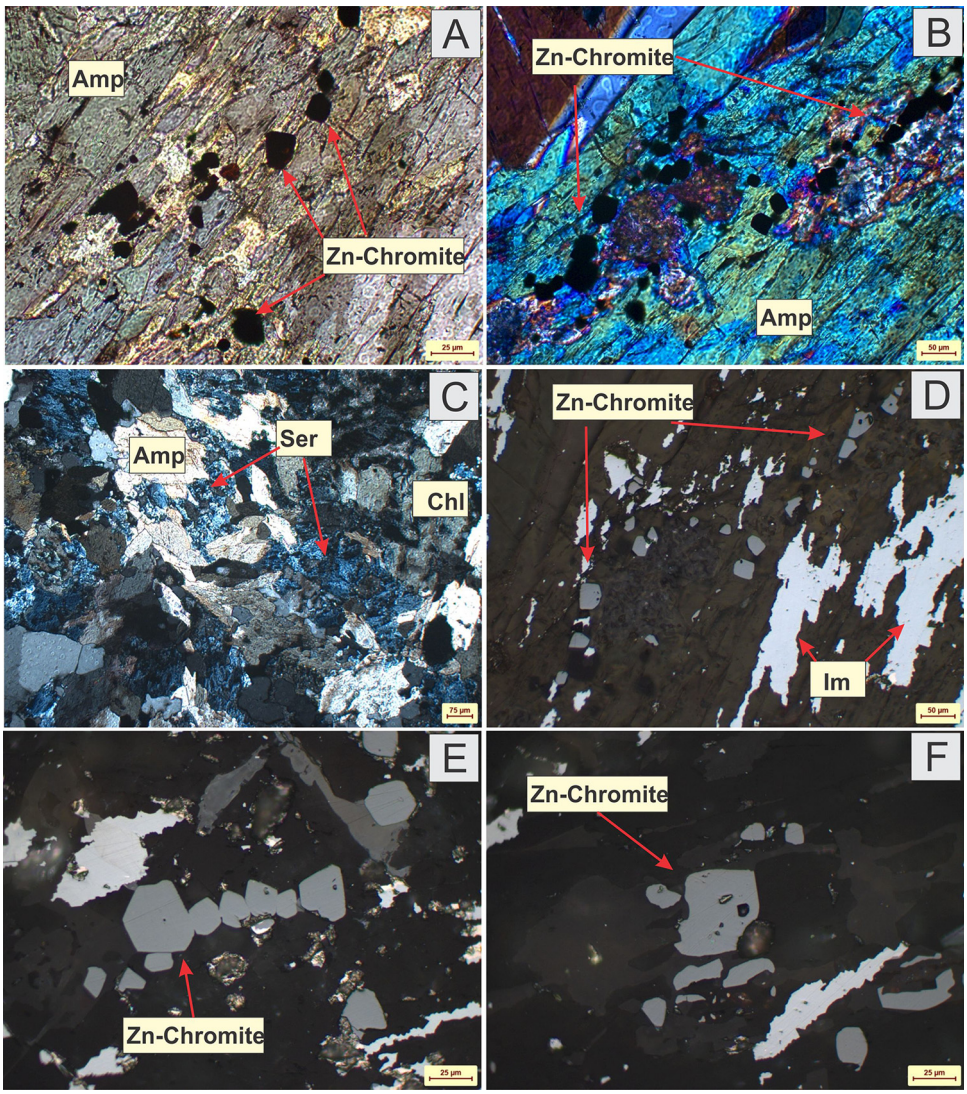

Fig. 3 **A** Photomicrograph of metapyroxenite showing the interlocking texture of clinopyroxene pseudomorph. **B** Representative BSE images indicating an elemental map of zincian chromite. These basic maps show homogeneous distribution and enrichment of Fe and Zn within chromite and don't follow any type of zoning pattern. **A–C** Representative photomicrographs of ultramafic xenoliths with the presence of zincian chromite. **D–F** Representative ore microscopic photographs of zincian chromite in oil immersion in reflected light. **G** Representative backscattered images and Fe–Cr-Zn-Mg–Al-Si elemental mapping of zincian chromite grain

check the distribution of the elements in SEM. As the rock is altered and metamorphosed, the analysed phases also show the effect of alterations. In most cases, several analyses were made on mineral grains, and those analytical compositions with totals close to 100% and a satisfactory structural formula were selected as representatives (Tables 1, 2, and 3). The representative analysis is further used to understand the effect of post-magmatic changes and the substitution of different elements during this effect. The fresh chromite composition by Manu Prasanth et al. (2017) was also included from SGB for comparison, consistent with the range of primary magmatic crystallisation.

4.2.1 Chromite

The analysed zincian chromite is euhedral to subhedral in shape, has smooth grain boundaries, and occurs as fine dissemination within metapyroxenite. It shows compositional variation due to various degrees of alteration (Barnes and Roeder 2001; Evans 2015, 2017).

Zincian chromite shows range of Cr_2O_3 varies from 39.69 wt% to 51.66 wt%, Al_2O_3 contents range from 5.30 wt% to 8.71 wt%, FeO contents range from 21.74 wt% to 27.51 wt%, Fe_2O_3 contents range from 10.19 wt% to 19.36 wt%, ZnO contents range from 1.73 wt% to 4.08 wt%, TiO_2 contents range from 0.23 wt% to 0.78 wt%, and MgO ranges from 0.07 wt% to 0.34 wt% (Table 1). Consequently, their Cr# [Cr/(Cr + Al)] shows a very narrow but high range from 0.83 to 0.85, whereas Mg# [Mg/(Mg + Fe^{2+})] shows a wide range from 0.38 to 0.89. The MnO and NiO contents are negligible and insignificant in zincian chromite. The calculated melt composition of Al_2O_3 and (FeO/MgO) by Maurel and Maurel (1982) ranges from 7.14 to 9.80 and 2.44 to 2.60 and TiO_2 by Kamenetsky et al. (2001) ranges from 0.35 to 0.97 (Table 1).

Fig. 3 continued

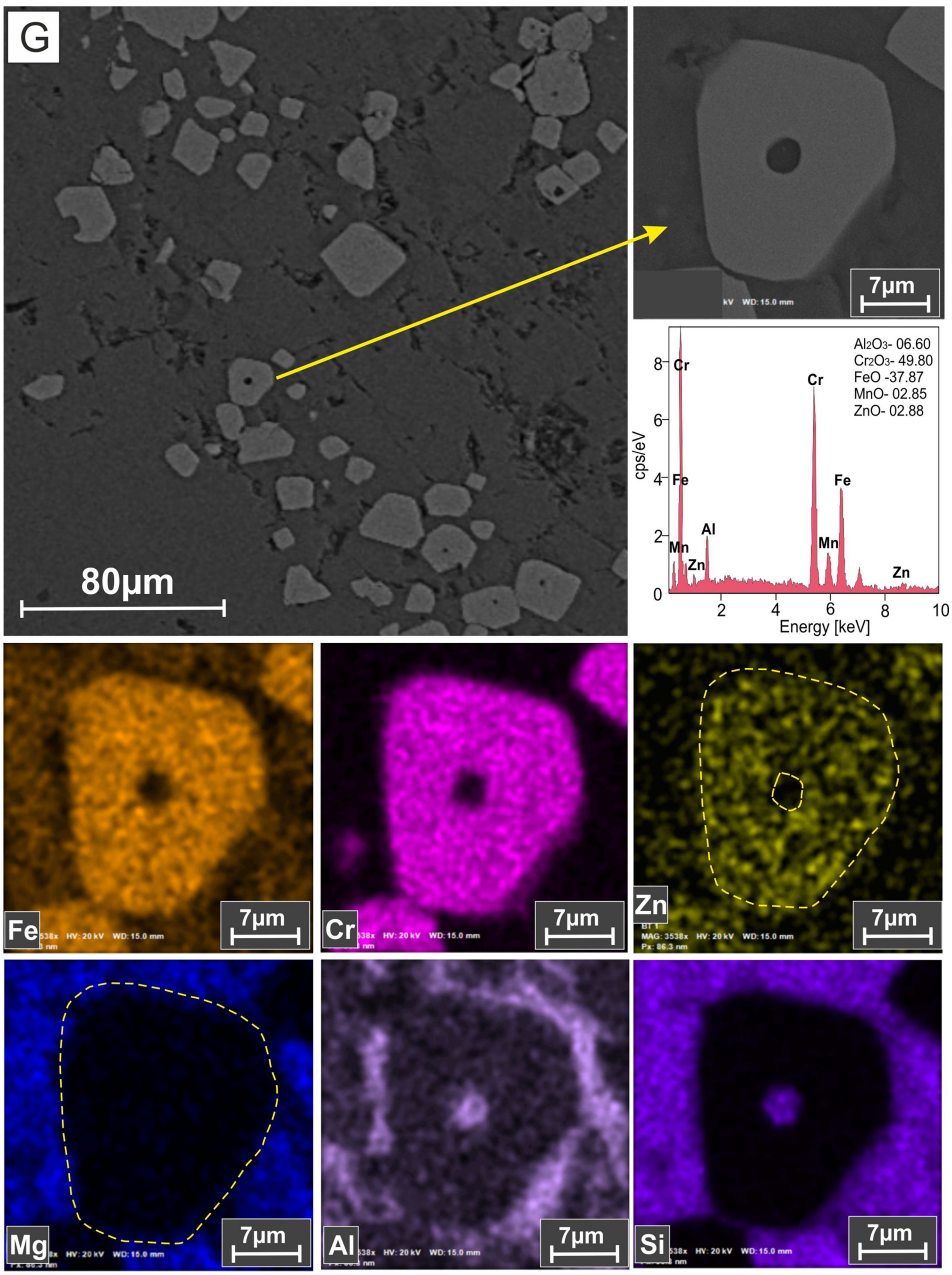

Zincian chromite is plotted in the Cr–Al–Fe^{3+} diagram and saddle between the Al-chromite and Fe-chromite composition but shows an affinity towards the Fe-chromite field (Fig. 4A). Subsequently, zincian chromite composition is also compared with the Cr–Al–Fe^{3+} compositions of spinels from different metamorphic facies (Purvis et al. 1972; Evans and Frost 1975; Freitas Suita and Strieder 1996), as well as with spinel stability limit (Sack and Ghiorso 1991; Barnes 2001) (Fig. 4A). Simultaneously, all zincian chromite falls in the field of spinel metamorphosed in the upper greenschist facies, at temperatures within 500 °C, which also shows an affinity towards the amphibolite facies spinel field. This result is consistent with Fig. 4B of Mg# (Mg/Mg + Fe^{2+}) vs Cr# (Cr/Cr + Al) where zincian chromite plots near the field of amphibolite or metamorphic field (Pober and Faupl 1988; Sack and Ghiorso 1991; Dupuis and Beaudoin 2011; Dill et al. 2021).

4.2.2 Pyroxene

Clinopyroxene is the dominant mineral phase within metapyroxenite, which shows significant alteration. The orthopyroxenes are present in subordinate amounts, and both pyroxenes occur as pseudomorph phases. The (clino- and ortho-) have restricted variation in composition, which

Table 1 Representative electron probe micro analysis data of zincian chromite from ultramafic xenolith

	PS-6.1	PS-6.2	PS-6.3	PS-6.4	PS-6.5	PS-6.6	PS-6.7	PS-6.8	PS-6.9	PS-6.10
TiO_2	0.56	0.44	0.48	0.46	0.53	0.40	0.43	0.36	0.29	0.23
Al_2O_3	6.03	5.82	6.12	6.34	5.97	5.95	5.99	5.76	6.13	5.89
Cr_2O_3	49.77	50.22	50.35	50.34	50.14	50.95	50.30	50.53	51.38	51.66
FeO^T	37.06	36.61	36.25	36.56	37.26	35.95	36.33	36.12	33.50	33.12
MnO	0	0	0.00	0.00	0.00	0.00	0.00	0.00	0.00	0.00
MgO	0.08	0.09	0.11	0.11	0.10	0.10	0.12	0.11	0.07	0.08
ZnO	3.16	3.08	3.44	3.29	3.17	3.27	3.55	3.16	4.08	4.01
NiO	0	0.01	0.04	0.00	0.05	0.01	0.00	0.00	0.01	0.01
Total	96.66	96.27	96.79	97.10	97.22	96.63	96.72	96.04	95.46	95.00
Fe_2O_3	12.39	12.06	12.40	12.13	12.62	11.75	12.75	12.30	11.66	11.38
FeO	24.67	24.55	23.85	24.44	24.64	24.20	23.58	23.82	21.84	21.74
Total	96.58	96.63	96.64	96.98	97.32	96.91	96.33	96.96	95.39	94.21
Ti	0.02	0.01	0.01	0.01	0.01	0.01	0.01	0.01	0.01	0.01
Al	0.27	0.26	0.27	0.28	0.26	0.27	0.27	0.26	0.28	0.27
Cr	1.49	1.51	1.50	1.50	1.49	1.52	1.51	1.52	1.56	1.58
Fe^{+3}	0.35	0.34	0.35	0.34	0.36	0.33	0.36	0.35	0.34	0.33
Fe^{+2}	0.78	0.78	0.75	0.77	0.78	0.77	0.75	0.76	0.70	0.70
Mn	0.00	0.00	0.00	0.00	0.00	0.00	0.00	0.00	0.00	0.00
Mg	0.00	0.01	0.01	0.01	0.01	0.01	0.01	0.01	0.00	0.00
Ni	0.00	0.00	0.00	0.00	0.00	0.00	0.00	0.00	0.00	0.00
Zn	0.02	0.02	0.02	0.02	0.02	0.02	0.02	0.02	0.02	0.02
FeO/MgO	0.55	0.46	0.51	0.55	0.51	0.52	0.56	0.53	0.81	0.56
Al_2O_3 melt	7.84	7.65	7.92	8.11	7.78	7.77	7.80	7.59	7.93	7.71
TiO_2 melt	0.74	0.61	0.65	0.63	0.71	0.56	0.60	0.52	0.43	0.36
Cr#	0.85	0.85	0.85	0.84	0.85	0.85	0.85	0.85	0.85	0.85
Mg#	0.01	0.01	0.01	0.01	0.01	0.01	0.01	0.01	0.01	0.01
	PS-6.11	PS-6.12	PS-6.13	PS-6.14	PS-6.15	PS-6.16	PS-6.17	PS-6.18	PS-6.19	PS-6.20
TiO_2	0.40	0.27	0.33	0.27	0.40	0.44	0.49	0.44	0.78	0.70
Al_2O_3	5.70	5.62	5.63	5.30	6.08	5.96	6.15	6.07	6.40	6.35
Cr_2O_3	50.59	50.70	50.64	50.56	51.40	51.30	51.57	51.12	50.00	51.14
FeO^T	36.02	36.59	36.87	36.75	34.12	34.51	34.59	35.17	35.96	34.53
MnO	0.00	0.00	0.00	0.00	0.00	0.00	0.00	0.00	0.00	0.00
MgO	0.11	0.13	0.10	0.12	0.14	0.15	0.17	0.16	0.12	0.08
ZnO	3.22	3.17	2.90	2.88	3.50	3.62	3.08	3.11	3.45	3.63
NiO	0.00	0.02	0.00	0.03	0.04	0.06	0.05	0.04	0.00	0.03
Total	96.04	96.50	96.47	95.91	95.68	96.04	96.10	96.11	96.71	96.46
Fe_2O_3	11.94	12.45	11.94	12.19	10.90	11.51	10.19	10.87	11.75	10.92
FeO	24.08	24.14	24.93	24.56	23.22	23.00	24.40	24.30	24.21	23.62
Total	95.99	96.23	96.45	96.53	95.80	95.50	96.13	96.45	96.89	95.51
Ti	0.01	0.01	0.01	0.01	0.01	0.01	0.01	0.01	0.02	0.02
Al	0.26	0.25	0.25	0.24	0.27	0.27	0.28	0.27	0.28	0.28
Cr	1.53	1.52	1.52	1.53	1.55	1.54	1.55	1.54	1.49	1.53
Fe^{+3}	0.34	0.36	0.34	0.35	0.31	0.33	0.29	0.31	0.33	0.31
Fe^{+2}	0.77	0.77	0.79	0.79	0.74	0.73	0.77	0.77	0.76	0.75
Mn	0.00	0.00	0.00	0.00	0.00	0.00	0.00	0.00	0.00	0.00
Mg	0.01	0.01	0.01	0.01	0.01	0.01	0.01	0.01	0.01	0.00
Ni	0.00	0.00	0.00	0.00	0.00	0.00	0.00	0.00	0.00	0.00
Zn	0.02	0.02	0.02	0.02	0.02	0.02	0.02	0.02	0.02	0.02

Table 1 continued

	PS-6.11	PS-6.12	PS-6.13	PS-6.14	PS-6.15	PS-6.16	PS-6.17	PS-6.18	PS-6.19	PS-6.20
FeO/MgO	0.51	0.53	0.58	0.56	0.49	0.56	0.57	0.56	0.53	0.57
Al_2O_3 melt	7.54	7.46	7.47	7.15	7.88	7.78	7.94	7.87	8.16	8.12
TiO_2 melt	0.56	0.41	0.48	0.41	0.56	0.61	0.67	0.61	0.98	0.89
Cr#	0.86	0.86	0.86	0.86	0.85	0.85	0.85	0.85	0.84	0.84
Mg#	0.01	0.01	0.01	0.01	0.01	0.01	0.01	0.01	0.01	0.01

commonly confirms the clinoferrosilite in clinopyroxene and saddle between diopside to hedenbergite in orthopyroxenes, according to the classification by Morimoto (1989) (Fig. 4C). They also plot in the experimentally contoured Ca–Mg–Fe phase-relation diagram at 1.0 GPa (after Lindsley 1983) shows their position below the range of 700 °C temperature (Fig. 4C).

The clinopyroxene shows a very restricted range but high values of SiO_2 (50.53–51.34 wt%), CaO (20.49–22.69 wt%), FeO^t (16.21–17.75 wt%), and MgO (8.61–9.24 wt%). Whereas, Al_2O_3 ranges from (0.39–0.86 wt%), TiO_2 (0.05–0.27 wt%), and Na_2O (0.16–0.2 wt%), which are meagre in proportion. The Mg number of clinopyroxene is medium and varies from 0.52 to 0.55.

The orthopyroxenes also show a very restricted range of SiO_2 (48.79–49.23 wt%), FeO^t (37.48–38.99 wt%) and MgO (10.27–10.80 wt%). Whereas, Al_2O_3 ranges from (0.26–0.43 wt%), CaO (0.51–1.13 wt%), and d TiO_2 (0.01–0.16 wt%), which are minor in proportion. The Mg number of orthopyroxene is a little higher than clinopyroxene and varies from 0.62 to 0.66.

4.2.3 Amphibole

The amphibole is also the dominant mineral phase in metapyroxenite, like pyroxenes. It is a product of the metamorphic alteration of pyroxene. The amphibole composition indicates two types of variation. Type-I is MgO–FeO rich, while type-II is CaO rich. Which typically supports they are alteration products of both clino- and orthopyroxenes. The classification diagram after Leake et al. 1977, shows the anthophyllite and ferro-hornblende composition of amphiboles (Fig. 4D). They are also plotted in the (Ca + Na + K) vs Si (apfu) diagram after Giret et al. (1980) to understand their nature. All amphibole compositions are plotted in the metamorphic field (Fig. 4D).

The amphibole$_{(type\text{-}I)}$ shows a narrow range but high values of SiO_2 (51.46–52.39 wt%), FeO^t (31.53–32.92 wt%), and MgO (10.58–11.61 wt%). Whereas, Al_2O_3 ranges from (0.11–0.70 wt%), CaO (0.38–1.70 wt%), and TiO_2 (up to 0.12 wt%), which are less in proportion. The Mg number of amphibole$_{(type\text{-}I)}$ is high and varies from 0.49 to 53.

In contrast, the amphibole$_{(type\text{-}II)}$ has a high range of SiO_2 (44.07–47.17 wt%), CaO (10.96–11.17 wt%), FeO^t (21.76–22.09 wt%), Al_2O_3 (6.72–9.11 wt%), MgO (7.54–8.92 wt%) and TiO_2 (0.40–1.75 wt%). It contains a minor K_2O ranging from (0.25–0.57 wt%) and Na_2O (0.83–1.25 wt%). The Mg number of amphibole$_{(type\text{-}II)}$ is medium and varies from 0.39 to 43.

5 Discussion

5.1 Nature and origin of zincian chromite in ultramafic xenoliths

Zincian spinels (gahnite) and silicates (staurolite, garnet) reported from the metamorphosed copper–lead–zinc deposits of different parts of the world mostly formed by desulphidation of sphalerite or direct crystallisation from hydrothermal fluids (Dill 2010, Ghosh et al. 2011; Dill et al. 2021, Baswani et al. 2022). Nevertheless, the possible genesis of zincian chromite different theories are proposed, i.e., primary magmatic (inclusions in diamonds and silicates) and post magmatic (alteration due to metamorphism or hydrothermal fluids rich in Zn content) (Paktunc and Cabri 1995; Gaetani and Grove 1997; Righter 2003; Downes et al. 2004; Gahlan et al. 2006; Gahlan and Arai 2007; Yang et al. 2007; Lagos et al. 2008; Arai and Ishimaru 2011; Fanlo et al. 2015). The primary magmatic zincian chromite is present as inclusions in a diamond within kimberlites and lamprophyres and also as small inclusions in silicate within meteorites (especially iron meteorites). The zincian chromite inclusion in diamonds can be distinguished from common chromite by high Mg# (0.3 to 0.8). The zincian chromite has extremely low Mg# (< 0.03), but both primary inclusions have a very low content of Fe^{3+}. Commonly found Mg − rich chromite inclusions in diamonds contain a low amount of Zn and Mn, and are assigned to the peridotitic paragenesis, together with olivine, pyroxene, and garnets (e.g., Tappert et al. 2005). Likewise, the origin of zincian chromite inclusions is possibly related to the recycling of previously altered/

Table 2 Representative electron probe micro analysis data of pyroxene from ultramafic xenolith

CaO	21.6	21.65	21.98	20.95	21.3	22.23	21.36	21.37	21.55	21.97	21.75	
Na_2O	0.22	0.25	0.26	0.23	0.23	0.23	0.22	0.18	0.22	0.24	0.22	
K_2O	0	0	0	0	0.01	0.01	0.01	0	0.01	0.01	0	
NiO	0	0.06	0.03	0	0	0.07	0.05	0	0	0.07	0.07	
Total	100.41	99.24	100.65	99.71	99.54	99.7	99.33	100.04	99.46	99.1	99.91	
Fe_2O_3	1.57	1.23	1.62	1.78	0.75	1.23	0.34	1.24	0.79	1.35	1.07	
FeO	16.08	15.71	15.73	16.15	16.46	15.10	16.31	16.33	16.07	15.23	16.27	
Total	100.567	99.364	100.812	99.888	99.615	99.823	99.364	100.164	99.539	99.235	100.017	
Si	1.97	1.97	1.97	1.96	1.98	1.97	1.98	1.97	1.98	1.97	1.97	
Ti	0.00	0.00	0.00	0.00	0.00	0.00	0.00	0.00	0.00	0.00	0.01	
Al	0.03	0.03	0.03	0.03	0.03	0.03	0.03	0.03	0.03	0.04	0.03	
Cr	0.00	0.00	0.00	0.00	0.00	0.00	0.00	0.00	0.00	0.00	0.00	
Fe^{+3}	0.05	0.04	0.05	0.05	0.02	0.04	0.01	0.04	0.02	0.04	0.03	
Fe^{+2}	0.52	0.51	0.51	0.52	0.54	0.49	0.53	0.53	0.52	0.50	0.53	
Mn	0.01	0.01	0.01	0.01	0.01	0.01	0.01	0.01	0.01	0.01	0.01	
Mg	0.51	0.51	0.51	0.53	0.51	0.52	0.52	0.52	0.52	0.51	0.50	
Ca	0.89	0.90	0.91	0.87	0.89	0.92	0.89	0.89	0.90	0.92	0.90	
Na	0.02	0.02	0.02	0.02	0.02	0.02	0.02	0.01	0.02	0.02	0.02	
K	0.00	0.00	0.00	0.00	0.00	0.00	0.00	0.00	0.00	0.00	0.00	
Ni	0.00	0.00	0.00	0.00	0.00	0.00	0.00	0.00	0.00	0.00	0.00	
Total	4.00	4.00	4.00	4.00	4.00	4.00	4.00	4.00	4.00	4.00	4.00	
XMg	0.50	0.50	0.50	0.50	0.49	0.51	0.50	0.50	0.50	0.51	0.49	
CaO	22.14	20.49	21.75	21.82	21.93	21.71	22.69	22.28	0.71	1.13	0.79	
Na_2O	0.23	0.2	0.24	0.22	0.21	0.24	0.16	0.21	0	0.09	0.02	
K_2O	0	0	0	0.01	0.01	0	0	0.01	0.01	0.02	0	
NiO	0.04	0.1	0	0	0	0	0	0.03	0.02	0.01	0.02	
Total	99.32	99.17	100.39	99.78	100.06	99.64	100.05	99.76	99.4	99.72	99.59	
Fe_2O_3	0.34	0.62	1.57	1.48	0.81	0.34	2.18	2.04	0.00	0.00	0.13	
FeO	15.78	16.85	15.85	15.42	15.58	16.29	14.49	14.71	37.88	37.51	37.89	
Total	99.354	99.232	100.547	99.929	100.141	99.674	100.269	99.964	99.400	99.720	99.603	
Si	1.98	1.98	1.97	1.97	1.98	1.98	1.96	1.96	1.99	1.99	1.99	
Ti	0.00	0.00	0.01	0.00	0.00	0.01	0.00	0.00	0.00	0.00	0.00	
Al	0.04	0.04	0.03	0.03	0.03	0.04	0.02	0.03	0.02	0.02	0.02	
Cr	0.00	0.00	0.00	0.00	0.00	0.00	0.00	0.00	0.00	0.00	0.00	
Fe^{+3}	0.01	0.02	0.05	0.04	0.02	0.01	0.06	0.06	0.00	0.00	0.00	
Fe^{+2}	0.51	0.55	0.51	0.50	0.50	0.53	0.47	0.48	1.29	1.27	1.29	
Mn	0.00	0.01	0.01	0.01	0.01	0.01	0.01	0.01	0.03	0.03	0.03	
Mg	0.51	0.53	0.52	0.52	0.53	0.51	0.52	0.52	0.64	0.63	0.64	
Ca	0.92	0.86	0.90	0.91	0.91	0.90	0.94	0.92	0.03	0.05	0.03	
Na	0.02	0.02	0.02	0.02	0.02	0.02	0.01	0.02	0.00	0.01	0.00	
K	0.00	0.00	0.00	0.00	0.00	0.00	0.00	0.00	0.00	0.00	0.00	
Ni	0.00	0.00	0.00	0.00	0.00	0.00	0.00	0.00	0.00	0.00	0.00	
Total	4.00	4.00	4.00	4.00	4.00	4.00	4.00	4.00	4.00	4.00	4.00	
XMg	0.50	0.49	0.50	0.51	0.51	0.49	0.53	0.52	0.33	0.33	0.33	
CaO	0.81	0.7	0.71	0.92	0.85	0.86	0.76	0.71	0.51	0.97	0.78	0.89
Na_2O	0.01	0.03	0	0	0	0	0	0.03	0.01	0.05	0.04	0
K_2O	0	0	0.01	0	0	0.01	0	0	0	0	0	0
NiO	0	0	0	0	0.04	0.01	0	0	0.07	0	0.02	0
Total	98.78	99.92	99.04	99.7	99.19	99.85	100.37	99.36	99.36	99.75	99.89	99.23

Table 2 continued

Fe_2O_3	0.00	0.00	0.00	0.17	0.00	0.51	0.72	0.00	0.00	0.21	0.23	0.00
FeO	37.59	38.55	38.12	37.81	37.71	37.47	38.34	37.85	38.09	37.96	37.74	37.48
Total	98.780	99.920	99.040	99.718	99.190	99.901	100.442	99.360	99.360	99.771	99.913	99.230
Si	2.00	2.00	1.99	1.99	1.99	1.98	1.98	2.00	2.00	1.99	1.99	1.99
Ti	0.00	0.00	0.00	0.00	0.00	0.00	0.00	0.00	0.00	0.00	0.00	0.00
Al	0.02	0.02	0.02	0.02	0.02	0.02	0.02	0.02	0.01	0.02	0.02	0.02
Cr	0.00	0.00	0.00	0.00	0.00	0.00	0.00	0.00	0.00	0.00	0.00	0.00
Fe^{+3}	0.00	0.00	0.00	0.01	0.00	0.02	0.02	0.00	0.00	0.01	0.01	0.00
Fe^{+2}	1.28	1.31	1.30	1.28	1.29	1.27	1.30	1.29	1.30	1.29	1.28	1.27
Mn	0.02	0.03	0.03	0.03	0.03	0.03	0.03	0.02	0.03	0.03	0.03	0.02
Mg	0.64	0.62	0.62	0.64	0.63	0.65	0.62	0.63	0.63	0.63	0.65	0.65
Ca	0.04	0.03	0.03	0.04	0.04	0.04	0.03	0.03	0.02	0.04	0.03	0.04
Na	0.00	0.00	0.00	0.00	0.00	0.00	0.00	0.00	0.00	0.00	0.00	0.00
K	0.00	0.00	0.00	0.00	0.00	0.00	0.00	0.00	0.00	0.00	0.00	0.00
Ni	0.00	0.00	0.00	0.00	0.00	0.00	0.00	0.00	0.00	0.00	0.00	0.00
Total	3.99	4.00	4.00	4.00	4.00	4.00	4.00	3.99	3.99	4.00	4.00	4.00
XMg	0.33	0.32	0.32	0.33	0.33	0.34	0.32	0.33	0.33	0.33	0.34	0.34

metamorphosed peridotites responsible for the generation of kimberlitic magma (Arai and Ishimaru 2011; Matsumoto et al. 2017).

The chromites in meteorites are commonly zincian and manganoan, which have relatively high Mg# and Cr#, ranging from 0.2 to 0.8 and > 0.8. This possibly indicates the equilibration of the Mg-bearing zincian chromite with some melt rich in Mg and siderophile elements at high temperature, which characteristically occur deep inside the early stage of Earth when the metallic core was formed (Yang et al. 2007). This has similarities with the origin of high Mg# chromite inclusions in diamonds. The Cr and Zn are slightly siderophile to chalcophile and may show similar behaviour in the silicate melts that are in equilibrium with the metallic core (Gaetani and Grove 1997; Righter 2003; Lagos et al. 2008). The possible origin of zincian chromite as inclusions in diamonds within kimberlites and the meteorite is unsuitable for the present study.

The next possible origin is post-magmatic due to alteration and metamorphism. The binary diagram (Fig. 5A−B) and ternary diagram (Fig. 5C) depicted the nature of the zincian chromite reported from the present study and support its metamorphic origin. The zincian chromite samples plot in the field of altered rock rather than inclusions in diamond, meteorites, and recycled mantle peridotites (Fig. 5) (Paktunc and Cabri 1995; Arai and Ishimaru 2011). Furthermore, it also suggests that they are the product of amphibolite grade of metamorphism than that of greenschist facies of metamorphism (Barnes et al. 2000) (Fig. 5C). To differentiate the zincian chromite origin and their grade of metamorphism samples were plotted in binary variation diagram in Fig. 6 (Barnes 2000). This strongly supports the amphibolite grade of metamorphism origin of zincian chromite than primary and altered greenschist facies.

Reported zincian chromite occurs as fine disseminations and thin bands in metapyroxenite xenoliths in host granite. They are euhedral to subhedral in shape and dominantly associated with amphibole and pyroxene. They show mutual boundary texture and development of triple junction 120° grain boundary contact with associated silicate. This texture is representative of the effect of high-grade metamorphism (Lewis et al. 2000), which is also get supported by the Al-Cr-Fe^{+3} diagram (Fig. 5C) and the metamorphic origin of amphibole from pyroxenes during prograde metamorphism (Fig. 4C − D). The enrichment of zinc in chromite during the present study considers due to metamorphic alteration as supported by the number of shreds of evidence. The evidence suggested that the zincian chromite-rich metapyroxenite is part of Bengpal supracrustal and occurs as xenoliths within granite/gneisses. In contrast, the SGB also contains the common Cr-rich and Zn-poor chromite in the main belt. The SGB has high Cr# (0.67–0.75) and moderate Mg# (0.11–0.5) values attributed to crystallisation from siliceous high-magnesium basalts (SHMB) magma in an island-arc setting (Manu Prasanth et al. 2017). The Fe^{3+}# (Fe^{3+}/(Fe^{3+} + Cr + Al) contents range from 0.06 to 0.15. Whereas zincian chromite has

Table 3 Representative electron probe micro analysis data of amphibole from ultramafic xenolith

	23/1	31/1	33/1	18/1	14/1	26/1	60/1	68/1
SiO_2	51.46	52.39	52.25	51.57	44.75	44.07	44.55	47.17
TiO_2	0.05	0	0.02	0.12	0.99	1.75	0.99	0.4
Al_2O_3	0.45	0.11	0.16	0.7	9.06	8.94	9.11	6.72
Cr_2O_3	0	0.01	0	0.02	0.03	0.05	0	0.01
FeO^T	32.92	31.53	32.11	32.25	21.77	22.09	21.76	22.08
MnO	0.58	0.57	0.53	0.59	0.18	0.19	0.15	0.19
MgO	11.06	11.61	11.02	10.58	7.75	7.54	7.73	8.92
CaO	0.6	0.59	0.38	1.7	11.17	11.11	11.12	10.96
Na_2O	0.08	0.05	0.06	0.05	1.19	1.25	1.16	0.83
K_2O	0.01	0.01	0	0.03	0.4	0.57	0.4	0.25
NiO	0	0	0	0	0	0	0	0
Total	97.21	96.87	96.53	97.61	97.29	97.56	96.97	97.53
Fe_2O_3	0	0	0	0	0.14	0	0	0
FeO	32.92	31.53	32.11	32.25	21.64	22.09	32.11	32.11
Total	97.21	96.87	96.53	97.61	97.30	97.56	107.32	107.56
Si	7.94	8.04	8.06	7.92	6.84	6.76	8.06	8.06
Ti	0.01	0.00	0.00	0.01	0.11	0.20	0.00	0.00
Al	0.08	0.02	0.03	0.13	1.63	1.62	0.03	0.03
Cr	0.00	0.00	0.00	0.00	0.00	0.01	0.00	0.00
Fe^{+3}	0.00	0.00	0.00	0.00	0.02	0.00	0.00	0.00
Fe^{+2}	4.25	4.05	4.15	4.14	2.77	2.83	4.15	4.15
Mn	0.08	0.07	0.07	0.08	0.02	0.02	0.07	0.07
Mg	2.54	2.66	2.54	2.42	1.77	1.72	2.54	2.54
Ca	0.10	0.10	0.06	0.28	1.83	1.83	0.06	0.06
Na	0.02	0.01	0.02	0.01	0.35	0.37	0.02	0.02
K	0.00	0.00	0.00	0.01	0.08	0.11	0.00	0.00
Ni	0.00	0.00	0.00	0.00	0.00	0.00	0.00	0.00
Total	15.02	14.96	14.93	15.01	15.43	15.47	14.93	14.93
Temp	365.92	#NUM!	304.73	437.46	701.19	810.50	304.73	304.73
XMg	0.37	0.40	0.38	0.37	0.39	0.38	0.38	0.38

high Cr# (0.83 to 0.85), Fe^{3+}# (0.14 to 0.17) and Mg# shows a wide range (0.38 to 0.89). The calculated parental melt composition of Al_2O_3 by Maurel and Maurel (1982) in main SGB chromite ranges from 10.75 to 12.52, whereas the zincian chromite from ultramafic xenoliths from 7.14 to 9.80. The TiO_2 composition in melt calculated by Kamenetsky et al. (2001) in the main SGB chromite ranges from 0.26 to 1.19, while in zincian chromite, it ranges from 0.35 to 0.97 (Table 1). This suggests that these two chromite has different origin in the Bastar craton as supported by their distinct spatial and temporal association. Their diverse nature and compositional variation are further supported in Fig. 7A , B.

All the compositional variations in the zincian chromite indicate that they deviate from common chromite that occurs in SGB and has a different post-magmatic alteration history, i.e., regional metamorphism. This is supported by the presence of ultramafic xenoliths within Bengpal gneisses that get exposed to regional metamorphism due to the heat generated and transformed during the emplacement of granitic magmatism. The global Neoarchaean magmatism followed by high-grade metamorphism is also supported by several studies in India and other parts of the world (Rajesham et al. 1993; Santosh et al. 2004; Jayananda et al. 2011). This metamorphic process may be a possible reason for zinc enrichment in chromite in the present study area. Similar Zn – rich chromites are reported from metamorphosed ultramafic rocks in the other part of the world (Thayer et al. 1964; Challis et al. 1995). Their Zn- enrichment occurred during the alteration/ metamorphism of olivine, pyroxene-rich rocks (Tappert et al. 2005; Matsumoto et al. 2017), which altered/metamorphosed to various degrees at low temperatures, i.e., mainly within the stability field of serpentine (Arai and Ishimaru 2011; Gahlan et al. 2006; Gahlan and Arai 2007; e.g., Proterozoic ophiolite of Bou Azzer, Morocco).

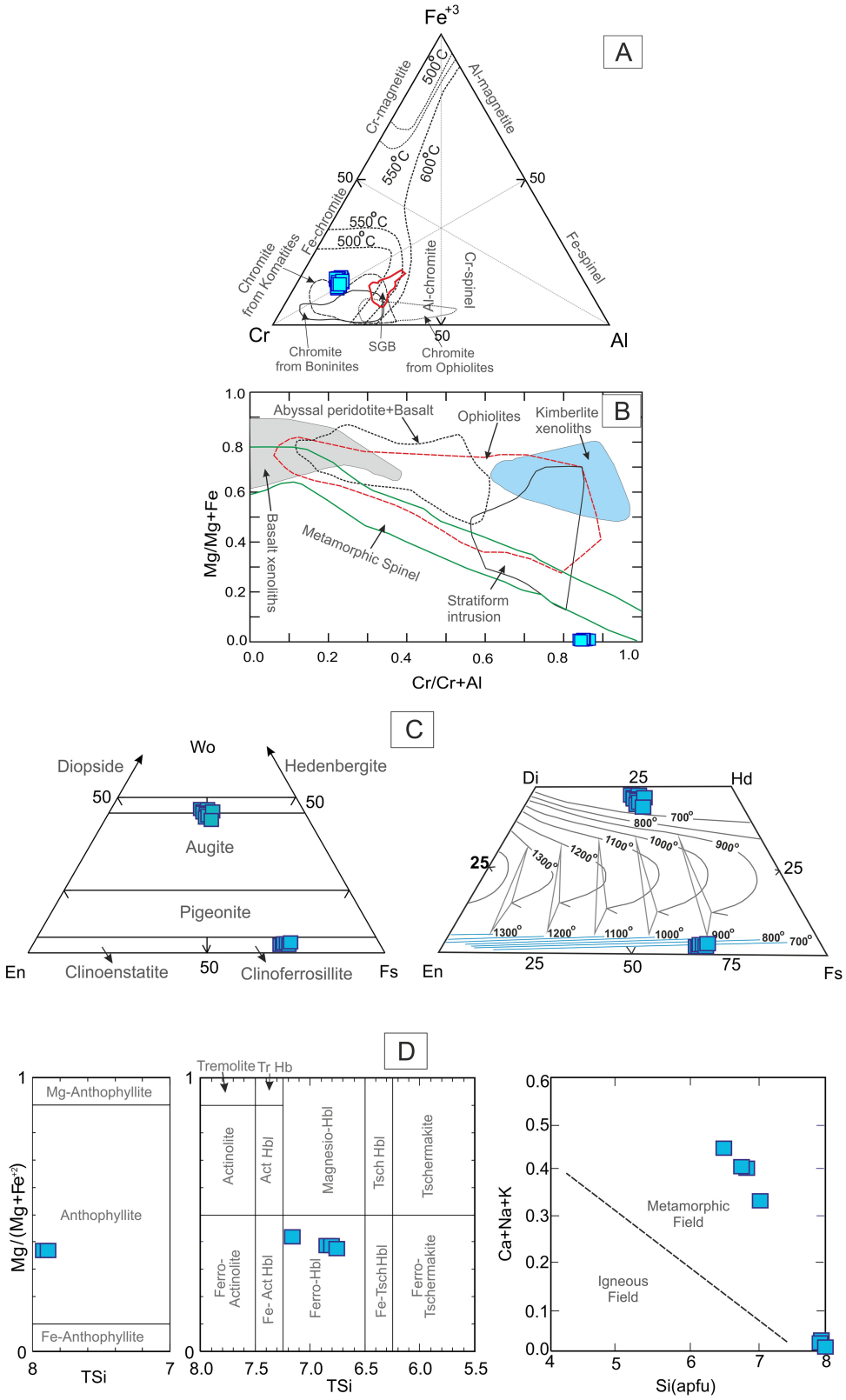

Fig. 4 **A** Cr-Al-Fe^{3+} diagram for mineral compositions of zincian chromite. Fields are after Barnes and Roeder (2001). **B** Zincian chromite plotted in the Cr-Mg–Al spinel and its source area (after Pober and Faupl 1988; Dupuis and Beaudoin 2011 and Dill et al. 2021). **C** Pyroxene composition from the zincian chromite-rich ultramafic in the classification diagram by Morimoto (1989), which also plotted in an experimentally contoured Ca–Mg–Fe phase-relation diagram at 1.0 GPa (after Lindsley 1983). **D** Nomenclature of amphibole after Leake et al. (1997), and amphiboles are plotted in the (Ca + Na + K) vs Si (apfu) diagram after Giret et al. (1980) to understand their nature

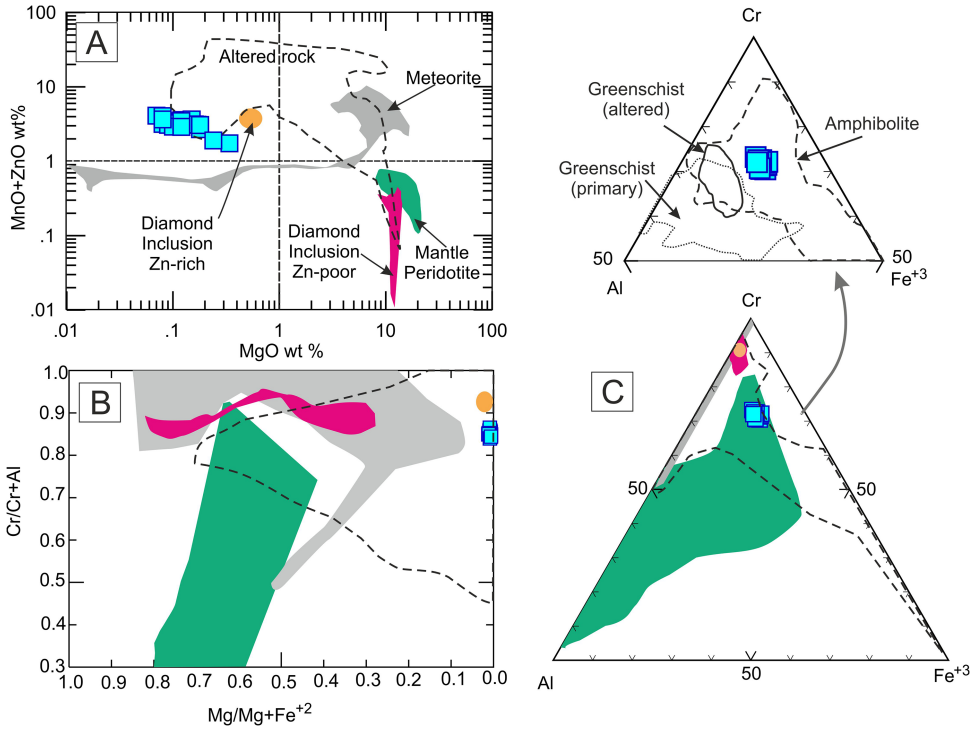

Fig. 5 **A** Relationship between (MnO + ZnO) and MgO contents of zincian chromite and related spinels. **B** Relationship between Cr/(Cr + Al) atomic ratio and Mg/Mg + Fe^{2+} ratio of zincian chromite and related spinels. **C** Relationship between Cr-Al-Fe^{3+} atomic ratio of zincian chromite and related spinels. Fields of different spinels were taken from Arai and Ishimaru (2011) and metamorphic fields were taken from Barnes (2000)

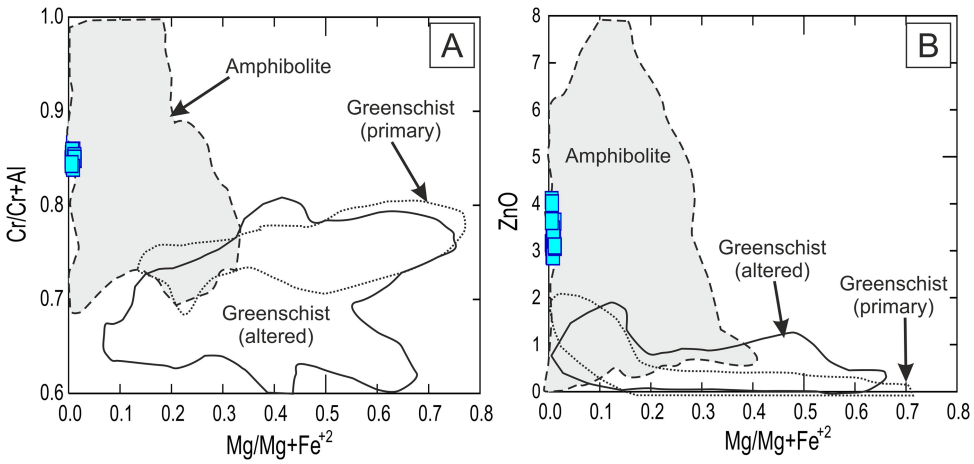

Fig. 6 Compositions of zincian chromite from ultramafic xenolith plotted against Mg/(Mg + Fe^{+2}). The field of chromite cores from amphibolite and greenschist facies terrains from Barnes 2000. Greenschist subdivided into 'primary' and 'altered' according to the nature of magnetite replacement

5.2 Enrichment of Zn- and Fe- in zincian chromite during metamorphic alteration

Chromite is highly susceptible to modification during early hydrous alteration and subsequent prograde metamorphism of host rocks (Barnes 2000). Barnes (2000) explains that the chromite compositions in komatiites are influenced by metamorphic processes, particularly above 500 °C. The studies of Evans & Frost (1975), Abzalov (1998), and Barnes (2000) highlighted two important effects of alteration commonly observed in chromite. First, chromites become rimmed and progressively replaced by chromian magnetite or 'ferritchromit'. Second, chromite core compositions become progressively modified during prograde metamorphism due to the exchange of components with surrounding silicate minerals. As a result of Mg–Fe exchange with silicates and carbonates. Chromite metamorphosed to amphibolite facies is enriched in Zn and Fe and depleted in Ni, relative to lower metamorphic grades (Barnes 2000). The observations reported here indicate that the process of Zn enrichment (1.73 to 4.08 wt%) is entirely secondary. Most of this chromite has a low Mg#, and some have relatively high Fe^{+3}#. In contrast, chromian spinel in the mantle peridotites exhibits a low ZnO content (< 0.4 wt%), though sometime Fe^{+3}# increases during metasomatism (Downes et al. 2004).

Significantly, high Zn contents above 1% are restricted to chromite undergoing metamorphic exchange.

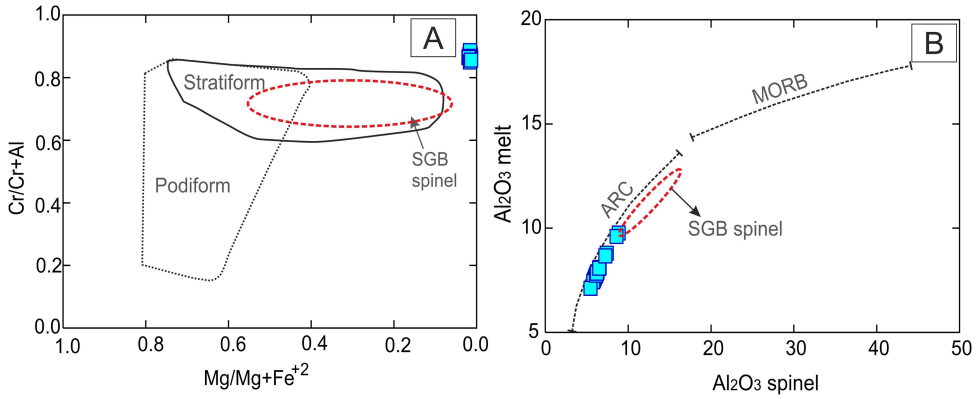

Fig. 7 A. Primary compositions of chromite from the Neoarchean Sonakhan Greenstone Belt in terms of their Cr# [(Cr/(Cr + Al)] versus Mg# [(Mg/(Mg + Fe^{2+})]. Podiform and stratiform fields are from Irvine (1967) and Leblanc and Nicolas (1992). B. Al_2O_3 melt versus Al_2O_3 zincian chromite of ultramafic enclaves and field of Sonakhan Greenstone Belt (SGB) chromites from Manu Prasanth et al. 2017. Data for mid-oceanic ridge basalts (MORB) and island arcs from Kamenetsky et al. (2001)

Furthermore, Zn contents over 2% are limited to the cores of chromite grains in amphibolite facies rocks (Figs. 5C and Fig. 6). They are never observed in primary greenschist facies chromite, whether in mineralised sequences or not (Barnes 2000). The olivine is the major repository for Mn, Zn, and Co in ultramafic rocks (chromian spinel can host up to 50% of bulk content; O'Reilly et al. 1997; De Hoog et al. 2010), and the availability of these elements in solution is the main factor controlling their incorporation in the lattice of chromian spinel (Sack and Ghiorso 1991), it should be expected that complete alteration of olivine would provide the necessary Mn, Zn and Co in the serpentinised peridotites occur worldwide (Paraskevopoulos and Economou 1981; Wylie et al. 1987; Bjerg et al. 1993; Challis et al. 1995; Liipo et al. 1995; Melcher et al. 1999; Tesalina et al. 2003; Downes et al. 2004; Pagé and Barnes 2009; Arai and Ishimaru 2011; Saumur and Hattori 2013; Singh and Singh 2013; Matsumoto et al. 2017), which is consistent with the present study. Matsumoto et al. (2017) discussed zinc enrichment in chromite within Nagasawa metaperidotites enclaves associated with sediments within host granites as a contact metamorphic event at ~ 500 °C due to hydrothermal circulation. They also suggest that the mobile zinc in these fluids was possibly derived from the thermally metamorphosed sediments adjacent to the granitic intrusion. The ultramafic has a spatial association with the meta-sedimentary rocks in the present study area. However, the clear field and petrographic evidence support the role of altered olivine for the source and mobility of Zn. The present study suggests that the transformation of common chromite to zincian chromite in altered/metamorphosed ultramafic xenolith due to the high grade of metamorphic exchange/transfer of Zn occurs during the emplacement of Neoarchaean granitic magmatism in the area (Fig. 8). However, the unusually high Mn, Zn, and Co contents in Bou-Azzer chromian spinels suggest that altering solutions should be anomalously rich in these metals (Gahlan and Arai 2007; Fanlo et al. 2015) and can be linked with polymetallic Cu-Pb–Zn mineralisation. In the present study, the zincian chromite is not enriched with Mn or Co; no such mineralisation is reported nearby. Therefore, there is a very rare possibility of mineralisation linked with the present study area.

6 Conclusion

The present study discussed the nature and origin of zincian chromite in the ultramafic xenoliths within Neoarchaean Bengpal gneisses from the Dongripali area, Bastar craton, Central India. The zincian chromite show high Cr#, Al, and Fe with significant Zn content, respectively. Such compositional variation generally represents their metamorphic origin rather than magmatic nature. The empirical thermometric calculation from chromite, amphibole, and pyroxene corroborated with the metamorphic nature. It attested to post-magmatic changes in ultramafic xenolith, form during low-P and high-T amphibolite grade facies of metamorphism (~ 700 °C). Neoarchaean granitic magmatism has played a vital role in generating and transferring heat during contact metamorphism with the hydration of ultramafic xenoliths and their serpentinisation. The olivine has a major repository for Mn, Zn, and Co in ultramafic; these elements get mobilised during the metamorphism and serpentinisation. This is a possible reason for the mobilisation of zinc and incorporation in chromite. As a result, chromite subjected to the metamorphic process gets enrichment of Zn and Fe due to elemental exchange. It converts to the zincian chromite as reported in altered ultramafics elsewhere.

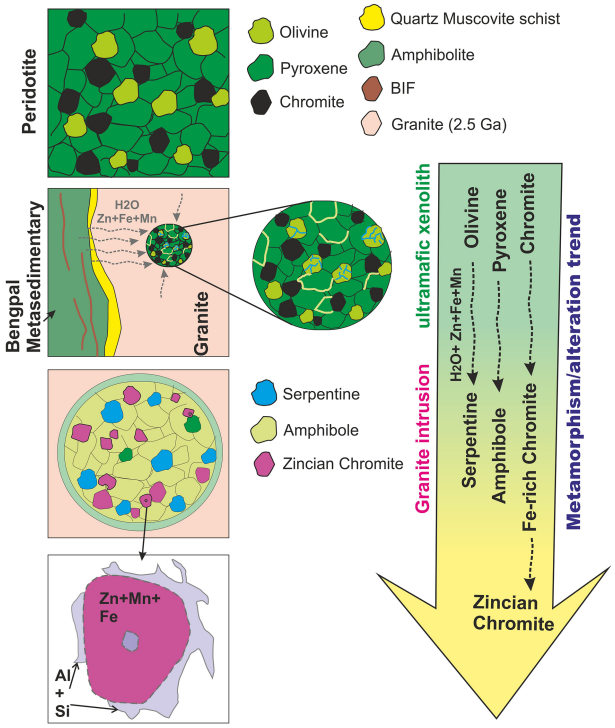

Fig. 8 A proposed cartoon diagram showing the relationship of ultramafic xenolith with granite magmatism in relevance to regional metamorphism and conversion of chromite to zincian chromite in the area

Acknowledgements The petrographic studies of zincian chromite rich ultramafic were carried out using LEICA DM RX at the Regional Petrology Laboratory, Geological Survey of India, Central Region, Nagpur, India. The silicate and oxide phases analyses were performed using a CAMECA SX-100 electron microprobe analyzer at the National Centre of Excellence in Geoscience Research (NCEGR), Geological Survey of India, Bangalore. The authors would like to express their sincere thanks to officials of the SEM, Palaeontology Laboratory, Geological Survey of India, Hyderabad and EPMA laboratory, NCEGR laboratory, Bangalore and the colleagues of GSI associated with exploration in the area. The authors also want to express their sincere thanks to Prof. Shoji Arai for discussion and critical comment to improve the manuscript in initial stage. The authors are thankful to Shri S. N. Mahapatro for his technical support. The authors acknowledge Geological Survey of India, Ministry of Mines, Government of India for funding the opportunity to work in this projects. Last but not the least the authors are thankful to Dr. Wubin Yang and anonymous reviewers for their critical review and constructive comments. The authors express sincere thanks to Dr. Binbin Wang, editor for providing opportunity and encouragement to submit the manuscript in the journal.

Declarations

Conflict of interest The authors declare that they have no conflict of interest.

References

Abzalov M (1998) Chrome-spinels in gabbro-wehrlite intrusions of the pechenga area, kola peninsula, russia: emphasis on alteration features. Lithos 43(3):109–134

Arai S (1992) Chemistry of chromian spinel in volcanic rocks as a potential guide to magma chemistry. Mineral Mag 56(383):173–184

Arai S, Ishimaru S (2011) Zincian chromite inclusions in diamonds: possibility of deep recycling origin. J Mineral Petrol Sci 106(2):85–90

Arai S, Yurimoto H (1994) Podiform chromitites of the tari-misaka ultramafic complex, southwestern Japan, as mantle-melt interaction products. Econ Geol 89(6):1279–1288

Armstrong JP, Barnett RL (2003) The association of Zn-Chromite with diamondiferous lamprophyres and diamonds: Unique compositions as a guide to the diamond potential of non-traditional diamond host rocks. vol 8

Barnes SJ, Roeder PL (2001) The range of spinel compositions in terrestrial mafic and ultramafic rocks. J Petrol 42(12):2279–2302

Baswani SR, Mishra BP, Mahapatro SN, Meshram T, Pati P, Md. Shareef, Korakoppa M, Mishra M, Md. Atif Raza, Roy S, Randive K, Malviya VP, Dora ML (2022) Petrochemical evaluation of gahnite from volcanogenic massive sulfide deposits in Betul belt, Central India: insight from petrography and in-situ trace element geochemistry. Geol J 1–22

Bjerg PL, Christensen TH (1993) A field experiment on cation exchange-affected multicomponent solute transport in a sandy aquifer. J Contam Hydrol 12(4):269–290

Bunch TE, Keil K, Olsen E (1970) Mineralogy and petrology of silicate inclusions in iron meteorites. Contrib Miner Petrol 25(4):297–340

Challis GA, Grapes RH, Palmer KJ (1995) Chromian muscovite, uvarovite, and zincian chromite; products of regional metasomatism in Northwest Nelson, New Zealand. Can Mineral 33:1263–1284

Chikami J, Miyamoto M, Takeda H (1999) The variation of Zn content in spinel group minerals and daubreelites of primitive achondrites. Antarct Meteor Res 12:139

Das AK, Khaoash S, Mishra P, Mohapatra BK, Mohanty J (2021) Chromite-bearing quartzite in the southern fringe of Singhbhum craton around Ghutrigaon Eastern India: Petrogenetic Implication. Geol J 56(7):3472–3496

Dick HJB, Bullen T (1984) Chromian Spinel as a Petrogenetic Indicator in Abyssal and Alpine-Type Peridotites and Spatially Associated Lavas. Contrib Miner Petrol 86(1):54–76

Dill HG (2010) The "chessboard" classification scheme of mineral deposits: Mineralogy and geology from aluminum to zirconium. Earth-Sci Rev 100:1–420

Dill HG, Balaban S-I, Buzatu A, Bornemann A, Techmer A (2021) The Quaternary volcanogenic landscape and volcaniclastic sediments of the Netherlands Antilles - markers for an in-active volcanic arc. Int J Earth Sci 111:149–172

Dora ML, Upadhyay D, Malviya VP, Meshram T, Baswani SR, Randive K, Meshram R, Suresh G, Naik R, Ranjan S (2021) Neoarchaean and Proterozoic crustal growth and reworking in the Western Bastar Craton, Central India: constraints from zircon, monazite geochronology and whole-rock geochemistry. Precambrian Res 362. https://doi.org/10.1016/j.precamres.2021.106284

Downes H (2004) Ultramafic Xenoliths from the Bearpaw Mountains, Montana, USA: Evidence for Multiple Metasomatic Events in the Lithospheric Mantle beneath the Wyoming Craton. J Petrol 45(8):1631–1662

Dupuis C, Beaudoin G (2011) Discriminant diagrams for iron oxide trace element fingerprinting of mineral deposit types. Miner Depos 46:319–335

Evans DM (2015) Metamorphic modifications of the muremera mafic-ultramafic intrusions, eastern burundi, and their effect on chromite compositions. J Afr Earth Sc 101:19–34

Evans DM (2017) Chromite compositions in nickel sulphide mineralized intrusions of the kabanga-musongati-kapalagulu alignment, east africa: petrologic and exploration significance. Ore Geol Rev 90:307–321

Evans BW, Ronald Frost B (1975) Chrome-spinel in progressive metamorphism—a preliminary analysis. Geochim Cosmochim Acta 39(6–7):959–972

Fanlo I, Gervilla F, Colás V, Subías I (2015) Zn-, Mn- and Co-rich chromian spinels from the Bou-Azzer Mining District (Morocco): constraints on their relationship with the mineralizing process. Ore Geol Rev 71:82–98

French JE (2008) U–Pb Dating of Paleoproterozoic Mafic Dyke Swarms of the South Indian Shield: Implications for Paleocontinental Reconstructions and Identifying Ancient Mantle Plume Events. PhD Thesis. University of Alberta. University of Alberta

Gaetani GA, Grove TL (1997) Partitioning of moderately siderophile elements among olivine, silicate melt, and sulfide melt: constraints on core formation in the Earth and Mars. Geochim Cosmochim Acta 61(9):1829–1846

Gahlan HA, Arai S (2007) Genesis of peculiarly Zoned Co, Zn and Mn-rich chromian Spinel in serpentinite of Bou-Azzer Ophiolite, Anti-Atlas, Morocco. J Mineral Petrol Sci 102(2):69–85

Gahlan HA, Arai S, Ahmed AH, Ishida Y, Abdel-Aziz YM, Rahimi A (2006) Origin of magnetite veins in serpentinite from the late Proterozoic Bou-Azzer ophiolite, anti-atlas, Morocco: an implication for mobility of iron during serpentinization. J Afr Earth Sc 46(4):318–330

Ghosh B, Thakur A (2011) Petrogenesis of Zincian spinel from mamandur base metal Sulphide Prospect, Tamil Nadu. J Geol Soc India 78:365–369

Ghosh JG (2004) 3.56Ga Tonalite in the central part of the bastar craton, India: Oldest Indian date. J Asian Earth Sci 23(3):359–64

Giret A, Bonin B, Leger J-M (1980) Amphibole compositional trends in oversaturated and undersaturated alkaline plutonic ring-composition. Can Mineral 18(4):481–495

González-Jiménez JM, Villaseca C, Griffin WL, Belousova E, Konc Z, Ancochea E, O'Reilly SY, Pearson NJ, Garrido CJ, Gervilla F (2013) The architecture of the European-mediterranean lithosphere: a synthesis of the Re-Os evidence. Geology 41(5):547–550

Groves DI, Barrett FM, Brotherton RH (1983) Exploration significance of chrome-spinels in mineralized ultramafic rocks and nickel-copper ores. Geol Soc s Afr Special Publication 7:21–30

Hill R, Roeder P (1974) The crystallisation of spinel from basaltic liquid as a function of Oxygen Fugacity. J Geol 82(6):709–729

Hoog De, Jan CM, Gall L, Cornell DH (2010) Trace-element geochemistry of mantle olivine and application to mantle petrogenesis and geothermobarometry. Chem Geol 270(1–4):196–215

Irvine TN (1965) Chromian spinel as a petrogenetic indicator: Part 1 Theory. Can J Earth Sci 2(6):648–672

Irvine TN (1967) Chromian Spinel as a Petrogenetic Indicator: Part 2. Petrologic Applications. Can J Earth Sci 4(1):71–103

Jayananda M, Moyen J-F, Martin H, Peucat J-J, Auvray B, Mahabaleswar B (2000) Late Archaean (2550–2520 Ma) Juvenile Magmatism in the Eastern Dharwar Craton, Southern India: Constraints from Geochronology, Nd–Sr Isotopes and Whole Rock Geochemistry. Precambr Res 99(3–4):225–254

Jayananda M, Banerjee M, Pant NC, Dasgupta S, Kano T, Mahesha N, Mahabaleswar B (2012) 2.62 Ga high-temperature metamorphism in the central part of the Eastern Dharwar Craton: Implications for Late Archaean tectonothermal history. Geol J 47(2–3):213–36

Johan Z, Ohnenstetter D (2010) Zincochromite from the Guaniamo River Diamondiferous Placers, Venezuela: Evidence of Its Metasomatic Origin. Can Mineral 48(2):361–374

Kamenetsky VS (2001) Factors controlling chemistry of magmatic spinel: an empirical study of associated Olivine, Cr-Spinel and melt inclusions from primitive rocks. J Petrol 42(4):655–671

Lagos M, Ballhaus C, Münker C, Wohlgemuth-Ueberwasser C, Berndt J, Kuzmin DV (2008) The Earth's missing lead may not be in the core. Nature 456(7218):89–92

Leake BE, Woolley AR, Arps CES, Birch WD, Gilbert MC, Grice JD, Hawthorne FC (1997) Nomenclature of amphiboles; report of the subcommittee on amphiboles of the international mineralogical association commission on new minerals and mineral names. Mineral Mag 61(405):295–310

Leblanc M, Nicolas A (1992) Ophiolitic Chromitites. Int Geol Rev 34(7):653–686

Lewis JL, Day SM, Magistrale H, Eakins J, Vernon F (2000) Regional crustal thickness variations of the Peninsular Ranges. Southern Calif Geol 28(4):303

Liipo J, Vuollo J, Nykänen V, Piirainen T, Pekkarinen L, Tuokko I (1995) Chromites from the early proterozoic outokumpu-jormua ophiolite belt: a comparison with Chromites from Mesozoic ophiolites. Lithos 36(1):15–27

Lindsley DH (1983) Pyroxene thermometry. Am Miner 68(5–6):477–493

Mahabaleswar B, Peucat JJ (1988) 2.9 b.y. Rb-Sr age of the granulite facies rocks of Satnur-Halagur and Sivasamudram Areas, Karnataka, South India. Geol Soc India 32(6):461–67

Manu Prasanth MP, Hari KR, Chalapathi Rao NV, Hou G, Pandit D (2018) An Island-Arc tectonic setting for the Neoarchean Sonakhan greenstone belt, Bastar craton, central India: insights from the chromite mineral chemistry and geochemistry of the siliceous high-Mg Basalts (SHMB). Geol J 53(4):1526–1542

Matsumoto I, Arai S, Miura M (2017) Chromian spinels and olivines in a contact-metamorphosed peridotitesediment system from Nagasawa, SW Japan: Implications for mobility of elements in a hydrothermal condition system. Ore Geol Rev 91:682–694

Maurel C, Maurel Etude P (1982) Expérimentale de La Distribution de l'aluminium Entre Bain Silicaté Basique et Spinelle Chromifère. Implications Pétrogénétiques: Teneur En Chrome Des Spinelles. Bulletin Minéralogie 105:197–202

Meert, Joseph G., Manoj K. Pandit, Vimal R. Pradhan, Jonathan Banks, Robert Sirianni, Misty Stroud, Brittany Newstead, and Jennifer Gifford (2010) Precambrian Crustal Evolution of Peninsular India: A 3.0 Billion Year Odyssey. J Asian Earth Sci 39 (6): 483–515.

Meshrama T, Dora ML, Baswani SR, Upadhyay D, Meshrama R, Randive K, Ranjan S, Nanda JK (2021) Petrogenesis and U\\Pb geochronology of charnockites flanking the Pranhita Godavari rift in peninsular India-link between the Bastar and Eastern Dharwar Cratons. Gondwana Res 92: 113–132

Melcher F, Grum W, Thalhammer TV, Thalhammer OAR (1999) The giant chromite deposits at Kempirsai, Urals: constraints from trace element (PGE, REE) and isotope data. Miner Deposita 34(3):250–272

Merlet C (1994) An accurate computer correction program for quantitative electron probe microanalysis. Mikrochim Acta 114–115(1):363–376

Merlet, Claude (1992) Quantitative electron probe microanalysis: New accurate Φ (Pz) description. In Electron Microbeam Analysis. Mikrochimica Acta. Vienna: Springer Vienna 12:107–15

Meshram T (2020) Mineralogical variation in platinum group element within altered chromitite of the kondapalli layered igneous complex (Southern India): implication on magmatic evolution and its petrogenetic significance. Ore Geol Rev 120:103398

Meshram T, Nannaware S, Mahapatro SN, Dora ML, Baswani S, Randive K (2022) Chromite composition and platinum-group element distribution in the proterozoic chimalpahad anorthosite complex, south India: implications for magmatic processes and discrimination of tectonic setting. Lithosphere: 1–24

Mohanty S (2015) Precambrian continent assembly and dispersal events of south Indian and east Antarctic shields. Int Geol Rev 57(16):1992–2027

Morimoto N (1989) Nomenclature of pyroxenes. Mineral J 14(5):198–221

O'Reilly SY, Chen D, Griffin WL, Ryan CG (1997) Minor elements in olivine from spinel Lherzolite xenoliths: implications for thermobarometry. Mineral Mag 61(405):257–269

Page P, Barnes S-J (2009) Using trace elements in Chromites to constrain the origin of podiform chromitites in the Thetford mines ophiolite, Quebec. Canada Economic Geology 104(7):997–1018

Paktunc AD, Cabri LJ (1995) A proton- and electron-microprobe study of gallium, nickel and zinc distribution in chromian spinel. Lithos 35(3–4):261–282

Paraskevopoulos GM, Economou M (1981) Zoned Mn-rich chromite from podiform type chromite ore in serpentinites of northern greece. Am Miner 66(9–10):1013–1019

Peucat JJ, Mahabaleswar B, Jayananda M (1993) Age of younger tonalitic magmatism and granulitic metamorphism in the South Indian Transition Zone (Krishnagiri Area); Comparison with older peninsular gneisses from the Gorur, Hassan Area. J Metamorph Geol 11(6):879–888

Peucat JJ, Bouhallier H, Fanning CM, Jayananda M (1995) Age of the holenarsipur greenstone belt, relationships with the surrounding gneisses (Karnataka, South India). J Geol 103(6):701–710

Pober E, Faupl P (1988) The chemistry of detrital chrome spinels and its implications for the geodynamic evolution of the Eastern Alps. Geol Rundsch 77:641–670

Purvis AC, Nesbitt RW, Hallberg JA (1972) The Geology of part of the carr boyd rocks complex and its associated Nickel mineralization, Western Australia. Econ Geol 67(8):1093–1113

Rajesh HM, Mukhopadhyay J, Beukes NJ, Gutzmer J, Belyanin GA, Armstrong RA (2009) Evidence for an early Archaean granite from Bastar Craton, India. J Geol Soc 166(2):193–196

Rajesham T, Bhaskar Rao Y, Murti K (1993) The karimnagar granulite terrane-a new sapphirine bearing granulite province, South India. Geol Soc India 41(1):51–59

Righter K (2003) Metal-silicate partitioning of siderophile elements and core formation in the early Earth. Annu Rev Earth Planet Sci 31(1):135–174

Roeder PL (1994) Chromite, from the fiery rain of chondrules to the Kilauea Iki Lava Lake. Can Mineral 32(4):729–746

Sack RO, Ghiorso MS (1991) Chromian spinels as petrogenetic indicators: thermodynamics and petrological applications. Am Miner 76(5–6):827–847

Santosh M, Yokoyama K, Acharyya SK (2004) Geochronology and tectonic evolution of karimnagar and bhopalpatnam granulite belts Central India. Gondwana Res 7(2):501–518

Santosh M, Tsunogae T, Yang C-X, Yue-Sheng Han KR, Hari MPM, Prasanth SU (2020) The bastar craton, central India: a window to archean – paleoproterozoic crustal evolution. Gondwana Res 79:157–184

Sarkar G, Corfu F, Paul DK, McNaughton NJ, Gupta SN, Bishui PK (1993) Early Archean Crust in Bastar Craton, Central India—a geochemical and isotopic study. Precambr Res 62(1–2):127–137

Saumur BM, Hattori K (2013) Zoned Cr-spinel and ferritchromite alteration in forearc mantle serpentinites of the Rio San Juan Complex Dominican Republic. Mineral Magaz 77(1):117–136

Singh RP, Dubey CS, Singh SK, Shukla DP, Mishra BK, Tajbakhsh M, Ningthoujam PS, Sharma M, Singh N (2013) A new slope mass rating in mountainous Terrain, Jammu and Kashmir Himalayas: application of geophysical technique in slope stability studies. Landslides 10(3):255–265

Stein HJ, Hannah JL, Zimmerman A, Markey RJ, Sarkar SC, Pal AB (2004) A 2.5 Ga porphyry Cu–Mo–Au deposit at Malanjkhand, central India: implications for Late Archean continental assembly. Precambrian Res 134(3–4):189–226

Suita F, De MT, Strieder AJ (1996) Cr-Spinels from Brazilian Mafic-ultramafic complexes: metamorphic modifications. Int Geol Rev 38(3):245–267

Tappert R, Stachel T, Harris JW, Muehlenbachs K, Ludwig T, Brey GP (2005) Subducting oceanic crust: the source of deep diamonds. Geology 33(7):565

Tesalina SG, Nimis P, Augé T, Zaykov VV (2003) Origin of chromite in mafic–ultramafic-hosted hydrothermal massive sulfides from the main Uralian Fault, South Urals. Russia Lithos 70(1–2):39–59

Thayer TP, Charles Milton JD, Jr HR (1964) Zincian Chromite from Outokumpu, Finland1. Am Mineral 49(9–10): 1178–83.

Weiser TW, Hirdes W (1997) Zinc-rich chromite from paleoproterozoic conglomerates at Tarkwa gold mine Ghana. Can Mineral 35(3):587–595

Wiedenbeck, M., J.N. Goswami, Roy A.B. (1996) Stabilisation of the Aravalli Craton of Northwestern India at 2.5 Ga: An Ion Microprobe Zircon Study. Chemical Geology 129(3–4):325–40.

Wylie AG, Candela PA, Burke TM (1987) Compositional zoning in unusual Zn-Rich chromite from the sykesville district of maryland and its bearing on the origin of 'Ferritchromit.' Am Miner 72(3–4):413–422

Yang J-S, Dobrzhinetskaya L, Bai W-J, Fang Q-S, Robinson PT, Zhang J, Green HW (2007) Diamond- and coesite-bearing chromitites from the luobusa ophiolite. Tibet Geol 35(10):875